Enhanced electrochemical etching of ion irradiated silicon by localized amorphization

Z. Y. Dang,[1] M. B. H. Breese,[1] Y. Lin,[2] E. S. Tok,[2] and E. Vittone[3]
[1]*Centre for Ion Beam Applications (CIBA), Department of Physics, National University of Singapore Singapore 117542*
[2]*Department of Physics, National University of Singapore, 2 Science Drive 3, Singapore 117542*
[3]*Physics Department, NIS Excellence Centre and CNISM, University of Torino, via Pietro Giuria 1, 10125 Torino, Italy*

(Received 11 March 2014; accepted 3 May 2014; published online 15 May 2014)

A tailored distribution of ion induced defects in p-type silicon allows subsequent electrochemical anodization to be modified in various ways. Here we describe how a low level of lattice amorphization induced by ion irradiation influences anodization. First, it superposes a chemical etching effect, which is observable at high fluences as a reduced height of a micromachined component. Second, at lower fluences, it greatly enhances electrochemical anodization by allowing a hole diffusion current to flow to the exposed surface. We present an anodization model, which explains all observed effects produced by light ions such as helium and heavy ions such as cesium over a wide range of fluences and irradiation geometries. © *2014 AIP Publishing LLC*. [http://dx.doi.org/10.1063/1.4876917]

Ion irradiation of semiconductors causes damage in which lattice atoms are displaced from their initial locations.[1–4] We previously showed how low fluence irradiation of p-type silicon with highly focused light ions, such as 30 keV helium, induces a "current funneling" effect[5,6] during subsequent electrochemical anodization.[7,8] For such low energy ions, the peak of defect density occurs very close to the irradiated surface.[9] A portion of these defects act as hole traps, resulting in the effective doping concentration being a minimum very close to the surface. During electrochemical anodization the diffusion component of the hole current is focused or "funneled" towards the surface along the gradient of reduced dopant density, resulting in a greatly enhanced local anodization current density,[5] formation of highly porous silicon, and enhanced photoluminescence.[6]

Simulations of the hole current flow during anodization predicted that high fluence irradiation (i.e., the fluence is high enough to stop anodization, producing surface or 3D silicon machined patterns after anodization) fully depletes the hole density within the irradiated volume;[5] no hole current flows through such a high resistivity volume during anodization, so it remains as crystalline silicon. For high ion energies of hundreds of keV, the maximum defect density is a few micrometers beneath the wafer surface; at shallower depths there lies a zone where the defect density is fairly uniform. Exclusion of hole current flow from the end-of-range peak containing a high defect density was demonstrated,[10,11] and the resultant buried silicon wires used to fabricate a variety of 3D micro- and nano-scale structures with applications in a variety of fields,[12–15] such as components for silicon photonics and for MEMS (microelectromechanical systems) and photonic lattices. However, for low ion energies, such as 30 keV helium, experimental results do not agree with simulations; instead, following anodization, a dip is observed at the center of lines irradiated at high fluences. Clearly, an additional factor contributes to anodization at high fluences, which is not accounted for in simulations, which assume that the irradiated volume remains fully crystalline. We show here that chemical etching of the localized, amorphized region induced by ion irradiation results in enhanced electrochemical anodization by enabling a hole current to flow, which would otherwise be prevented from passing through a depleted region. We combine effects due to chemical etching and electrochemical anodization of p-type silicon in a hydrofluoric acid (HF) electrolyte into a model, which describes all phenomena observed for 30 keV helium ion irradiation over a wide range of fluences and irradiation geometries. We demonstrate that this model can be used to predict and explain all anodization effects produced by low energy, heavy ion irradiation such as 15 keV cesium ions, which have a range of ~30 nm.

Fig. 1(a) shows the defect density produced by 30 keV helium ions in silicon, calculated using SRIM (Stopping and Range of Ions in Matter).[9] The ion range is about 450 nm, and for broad beam irradiation (i.e., the irradiated surface area is larger than the beam spreading at the end-of-range), the defect density profile peaks at ~250 nm beneath the surface. The defect density, and hence the majority carrier depletion, does not increase towards the surface, so there is no mechanism to induce a significant diffusion current towards it. For such broad beam irradiation, there is no lateral gradient of defect density, except at the edges of the irradiated region, so only here one observes a significant diffusion current flow, as observed in Ref. 6. In comparison, Figs. 1(b) and 1(c) show the defect distribution produced by the same ions focused to a small probe size of <1 nm in a helium ion microscope.[16] Under these conditions, there now exists a strong gradient of increasing defect density towards the surface so one expects a strong diffusion current funneled to the surface during electrochemical anodization, producing a dip owing to a faster etching rate. Comparison of the anodization behaviour of silicon irradiated in focused and broad beam geometries thus provides an insight into the significance of diffusion current funneling, since it is expected in the former irradiation geometry but absent in the latter. The same study

 © 2014 AIP Publishing LLC

This article is copyrighted as indicated in the article. Reuse of AIP content is subject to the terms at: http://scitation.aip.org/termsconditions. Downloaded to IP: 86.189.1.108 On: Fri, 16 May 2014 15:43:42

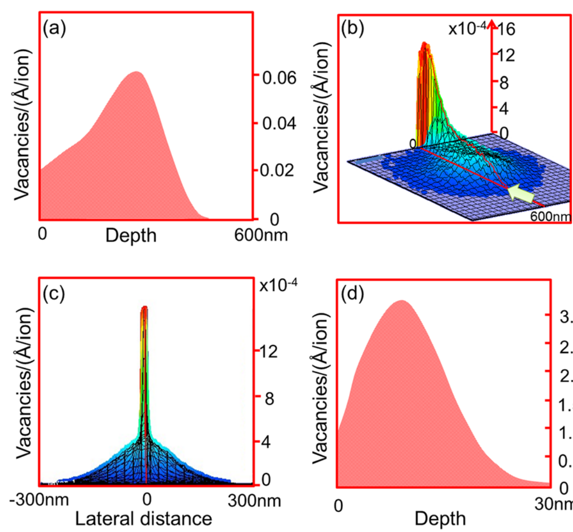

FIG. 1. SRIM calculation of defect density distribution in silicon: (a) 2D depth plot for 30 keV helium ions; (b) 3D plot for 30 keV helium ions; (c) Lateral distribution for 30 keV helium ions summed over all depths; (d) 2D depth plot for 15 keV cesium ions.

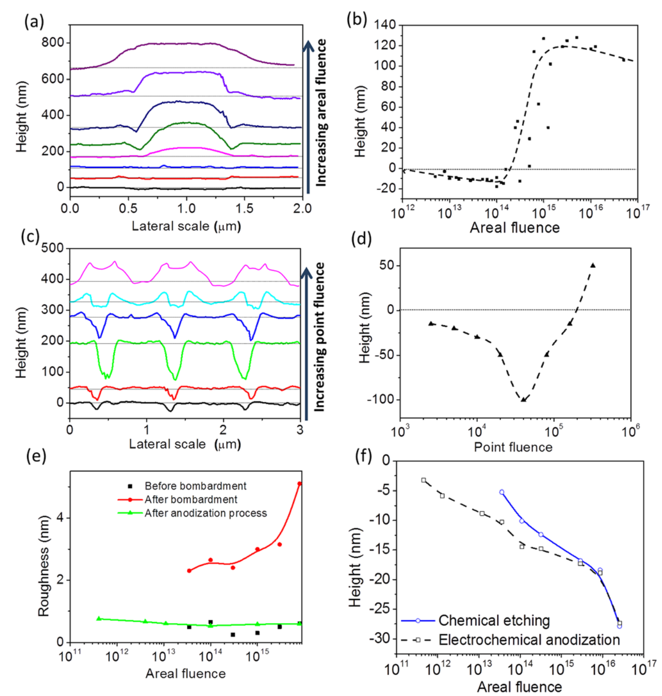

FIG. 2. 30 keV helium ion irradiation with a range of (a), (b) broad beam fluences over a $1 \times 1\,\mu m^2$ area, and (c), (d) point fluences with the beam focused to 1 nm, after anodization and removal of the porous silicon. In (a) the areal fluences are: 7.5×10^{13}, 1.3×10^{14}, 3×10^{14}, 1.3×10^{15}, 3×10^{15}, 1.2×10^{16}, and 5×10^{16}. (b) and (d) show the height at the center of the irradiated region relative to the unirradiated background, extracted from the line scans in (a) and (c), respectively, which are progressively offset on the vertical scale for clarity. (e) Surface roughness of regions irradiated with 15 keV cesium ions versus fluence, measured before and after ion irradiation, and also after anodization and porous silicon removal. (f) Step height after chemical, and then electrochemical etching of cesium irradiated regions versus areal fluence, data from AFM images. The units for areal fluence (ions/cm^2) and point fluence (ions/point) are omitted for clarity along the horizontal scales.

provides evidence of the importance of chemical etching superposed on the electrochemical anodization behavior in explaining effects, which cannot be explained using a model in which the lattice remains crystalline and the sole effect of ion irradiation is to deplete the irradiated volume.

A p-type silicon wafer resistivity of 0.4 Ω·cm wafer was chosen for this study, the same as that used in our previous observation of current funneling.[5,6] This wafer resistivity produces the full range of anodization effects due to ion irradiation over a range of fluences, which can be achieved in periods of minutes, rather than hours required for lower resistivity material, or over too short a difference in fluence to be easily controlled, as for higher resistivity wafers. After anodization, the porous silicon was removed by thermal oxidation, to convert it to oxidized porous silicon, which was removed by immersion in 2% HF (hydrofluoric acid).

Figs. 2(a) and 2(b) show the effects produced by broad beam irradiation over a $1 \times 1\,\mu m^2$ area. Fig. 2(a) plots the resultant vertical height across the anodized region for different areal fluences (units of ions/cm^2). All samples were electrochemically anodized at a current density of 60 mA/cm^2 in 24% HF. The anodization period was 3 s, producing an etch depth of the unirradiated background of ∼150 nm, significantly less than the ion range. Fig. 2(b) plots the height at the centre of the irradiated region versus fluence compared with the unirradiated background. At low fluences, the irradiated region has a shallow dip, consistent with a slightly increased current flow to the irradiated surface due to weak current funneling. With increasing fluence, the effective doping density of the irradiated volume decreases, and a barrier potential is progressively formed, which hinders the hole diffusion towards the surface, resulting in a reduced anodization rate compared to the unirradiated background, so forming a raised bump. The shallow dip surrounding the raised bump is consistent with the hole anodization current deflected around the irradiated volume since it cannot pass through it.[11] Above a fluence of $\sim 10^{16}$ ions/cm^2, the irradiated volume is fully depleted, and if the raised bump was influenced solely by anodization of fully crystalline silicon, its height should remain constant for higher fluences. However, the bump height decreases with fluence, suggesting an additional etching mechanism at work in this regime.

We compare this behaviour with that for same ions focused to a probe size of ∼1 nm. Fig. 3 shows AFM (atomic force microscope) images of the resultant features after anodization, and Figs. 2(c) and 2(d) show the corresponding line scans of the vertical height profile and the variation in height of the central irradiated region versus point fluence (i.e., number of ions per irradiated spot, assuming all ions are focused to a single point). Now a deep dip is observed at low point fluences, the maximum depth is more than 100 nm, compared to ∼10 nm for broad beam irradiation. This is because of the very large lateral and depth gradient of the defect density, Figs. 1(b) and 1(c), which induces a strong current funneling effect. At higher point fluences, Figs. 3(c) to 3(e), the dip becomes shallower and a concentric, raised ring where the anodization rate is lower than that of the background is observed at the surface around the irradiated spot. These portions of the irradiated volume are partially depleted and so transport a smaller hole current to the surface. The following question is important: the region inside this ring contains a higher defect density so is more depleted, so why is a dip rather than a bump still observed? For the highest point fluence, Fig. 3(f), a bump extending fully across the irradiated

This article is copyrighted as indicated in the article. Reuse of AIP content is subject to the terms at: http://scitation.aip.org/termsconditions. Downloaded to IP: 86.189.1.108 On: Fri, 16 May 2014 15:43:42

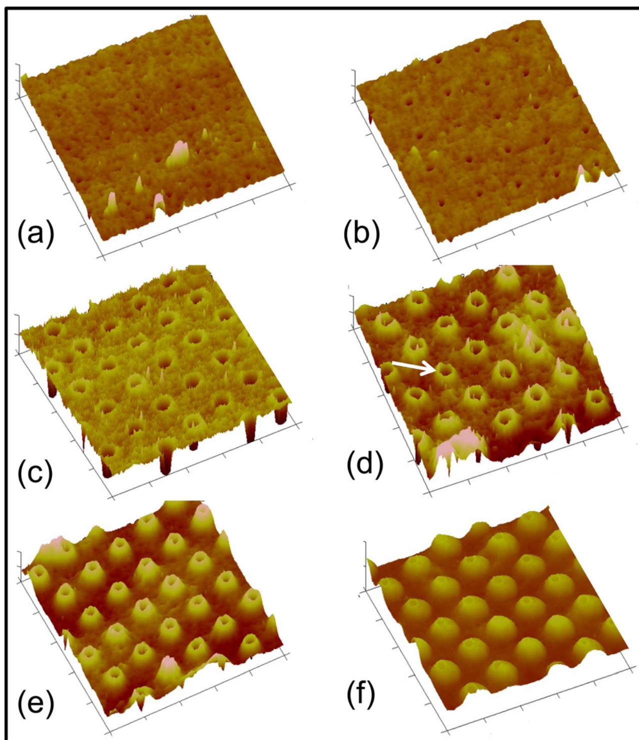

FIG. 3. AFM images of irradiated spotds with 30 keV helium ions, for a range of point fluences, after anodization and removal of the porous silicon. The spacing is a constant of 1 μm, the etch period is 3 s, and the etch depth of the unirradiated background is 150 nm. The fluences (ions/point) are: (a) 2.5×10^3, (b) 1×10^4, (c) 4×10^4, (d) 8×10^4, (e) 1.6×10^5, and (f) 3.2×10^5. See Fig. 2(c) for line scan profiles extracted from these images.

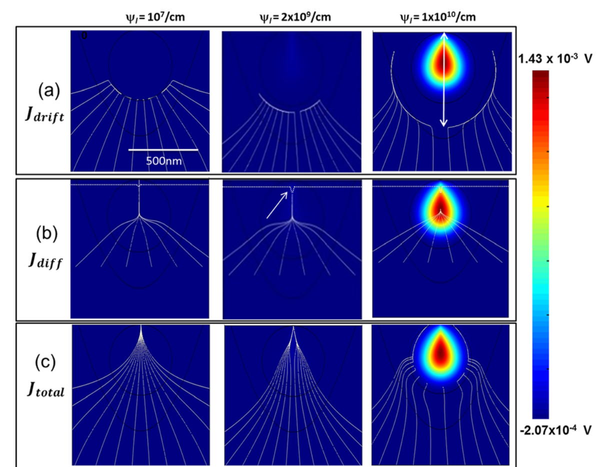

FIG. 4. Finite element method simulation results of anodization current distribution in Si with line irradiation with different line fluences (ψ_l, number of ions per cm of line length) of 30 keV helium ions: (a) drift current; (b) diffusion current; and (c) total current. The color scale indicates the potential height due to the depletion of the damaged region. The irradiated point is on the top surface of the blue square. In (b), the combined effect of anodization and chemical etching is indicated by the dashed white line. The arrow at $\psi_l = 2 \times 10^9$/cm indicates where chemical etching of the amorphized surface allows a diffusion current to flow, which would otherwise be absent.

region is indeed observed, though still with small dip of $\sim$30 nm in the middle. Now the central region behaves as though it is fully depleted, remaining unetched apart from the small central dip. Similar behaviour was observed for line irradiations over a range of fluence, not shown here.

We interpret the difference between the anodization behaviour at low damage levels between broad and focused beam irradiation as evidence that diffusion current funneling is an important mechanism where a strong gradient of defect density exists with depth and lateral position away from the point at which the surface was irradiated. Fig. 4 shows the separate drift and diffusion hole current components, calculated by the Finite Element Method, Ref. 5, flowing through and around an irradiated line, and also the total current, based on the defect distribution in Figs. 1(b) and 1(c). See Ref. 5 for more details of the simulation model, which is based on charge transport in irradiated silicon, which remains fully crystalline, though changes in mobility due to irradiation induced defects are accounted for. At low line fluences (defined as number of ions per centimeter of irradiated line length) ($\psi_l = 10^7$/cm), the drift current is repelled by the potential barrier at the irradiated region, while a large diffusion current flows towards the minimum dopant concentration at the surface. At high fluences, the holes can no longer cross the large potential barrier to reach the surface by diffusion, and the absence of any current flow predicts an unetched volume remaining after anodization, as in the raised bump in Fig. 3(f). However, these simulations do not explain the behaviour observed in Figs. 3(c) to 3(e) where there is a partially depleted concentric ring, which protrudes above the surface, surrounding a more depleted inner zone, which remains deeply etched. Neither do they explain the dip remaining at all irradiated spots and line irradiations at high fluences where no anodization current flows or for the small, but significant decrease in bump height at high fluence in Fig. 2(a) for broad beam irradiation.

This lack of agreement suggests that a model of electrochemical anodization due to ion induced changes in the local carrier distribution in a crystalline lattice is incomplete. We consider that the additional effect, which needs to be incorporated, is a low level of amorphization of the silicon lattice along the ion trajectory, which induces a chemical etching effect superposed on the electrochemical anodization. Such chemical etching of ion irradiated silicon and other semiconductors has been studied in Refs. 17–20. In Ref. 17, silicon was irradiated with high fluences of 30 keV helium ions, which converted the surface to an amorphous form, which was soluble in a 49% HF solution on soaking for 30 min. The lowest helium fluence at which etching was observed was $\sim 10^{14}/\mathrm{cm}^2$, equivalent to a vacancy density of $\sim 10^{20}/\mathrm{cm}^3$ from SRIM[9] at the surface. In this work we have used the term "fully crystalline" only in the sense that it is well below any structurally observable effects of amorphization, assumed to be around the same threshold of $10^{20}/\mathrm{defects/cm}^3$. Fig. 5(a) plots the relevant data from Ref. 17. In our study, a layer thickness of $\sim$150 nm is electrochemical anodized so the period is very short, in a solution of 24% HF, though the sample may be immersed in the HF solution for a few minutes prior to anodization. For such a short immersion period in a weaker HF solution, one expects thinner layers of a few tens of nanometres to be chemical etched away at high fluences. This is consistent with our observation of chemically etched dips up to 30 to 40 nm for the conditions used for anodization.

In a model incorporating all important effects of ion irradiation on the electrochemical anodization of silicon, it is

This article is copyrighted as indicated in the article. Reuse of AIP content is subject to the terms at: http://scitation.aip.org/termsconditions. Downloaded to IP: 86.189.1.108 On: Fri, 16 May 2014 15:43:42

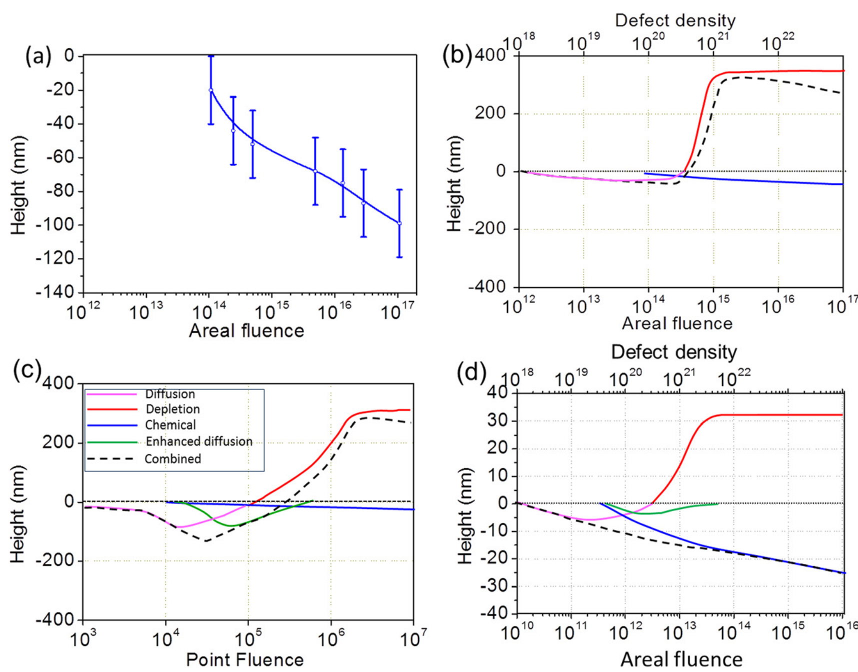

FIG. 5. (a) Chemically etched step height for increasing fluence of 30 keV helium ions, from Ref. 17. The rest of the figure shows a model of the different components which contribute to the anodization behaviour for (b) broad and (c) focused beam of 30 keV helium ions, and (d) broad beam of cesium ions. The key to the different colour lines for each figure is the same, shown in (c). The units for areal fluence (ions/cm^2) and point fluence (ions/point) are omitted for clarity along the horizontal scales.

necessary to include the effects of current funneling at low fluences and the depletion region at high fluences, lateral and depth variations of the defect density, and effects of chemical etching. We first consider 30 keV helium ions, which have a long range of hundreds of nanometers, well beyond what is removed by chemical etching or anodization. Figs. 5(b) and 5(c), respectively, show models for the various components of the anodization behavior versus fluence for broad beam and focused beam irradiation. The aim is to encompass the full span over which irradiation influences the observed etching behavior, so a direct comparison of the irradiation units on the horizontal axes in Figs. 5(b) and 5(c) for areal or point fluence is not necessary.

For broad beam irradiation, at low fluences current funnelling induces only a small enhanced anodization rate close to the surface before ion induced depletion of the full irradiated volume reduces and then fully stops the hole current flow at higher fluences. Chemical etching plays no significant role at low fluences; even if a few extra tens of nanometres of silicon are etched away, it does not result in modification of the anodization behaviour since no enhancement of the diffusion current flowing occurs because the defect peak lies beyond the etch depth. At high fluences chemical etching causes a reduction of the raised feature height since the ion induced defect density is significant—a fluence of 10^{16}/cm^2 is two orders magnitude above the amorphization threshold at which etching was first observed.[17] All aspects of this model are consistent with the behaviour shown in Fig. 2(b).

For focused beam irradiation, there is a strong effect of diffusion current funnelling, which produces a deep dip, becoming more pronounced with fluence. Chemical etching similarly results in the removal of irradiated material, having the strongest effect on the highest defect density close to the surface. Without this effect, the diffusion current would reduce with fluence as the irradiated zone closest to the surface becomes depleted, as for broad beam irradiation. Now, however, this effect is delayed at the central region since the most amorphized zone at the surface is chemically etched away, allowing a large diffusion current flow to persist from the less damaged material below. In Fig. 4, the etch front is indicated by the white dashed line; with increasing etch depth, the chemically induced dip allows an enhanced diffusion current to flow, which would otherwise be absent owing to the above depletion zone. Above a certain fluence, chemical etching cannot induce a further funnelling effect so the central region exhibits depletion behaviour, hence the raised bump in Fig. 3(f). A similar funnelling effect is not observed in the outer zone where a concentric raised ring occurs in Fig. 3, as there is a much weaker funnelling effect away from the irradiated spot. At high fluences, the height of the central part of the bump is reduced by chemical etching owing to the high localized defect density, hence the dip at the highest fluences for point irradiations in Fig. 3(f) and also for line irradiations.

A suitable test for this model is to predict and explain the anodization behaviour due to irradiation in other regimes of ion range and mass. We have studied whether similar changes in the electrochemical anodization behaviour of the irradiated volume can be induced with heavy ions such as cesium. This is commonly used to sputter material surfaces during sample preparation and thinning[20] using high fluences since the material removal rate is low, equivalent to removing $\sim$1 monolayer per 10^{15} ions/cm^2. We have irradiated with fluences of 10^{11} to 10^{16} ions/cm^2; we consider fluences of less than 10^{15} ions/cm^2 to be so low that little direct sputtering occurs. Heavy ions tend to produce amorphized zones along their trajectory,[21,22] and a wider mixture of defect types than light ions, so it is an interesting question as to whether they modify the anodization process in a similar manner to light ions. Fig. 1(d) shows the calculated defect density produced by 15 keV cesium ions; the defect profile peaks close to the surface and decreases to zero at a depth of about 30 nm. Only an order-of-magnitude estimate of the defect density is needed so we take no account of self-annealing, sputtering-induced changes to the profile, non-linear changes in the defect density versus fluence.[21,23]

This article is copyrighted as indicated in the article. Reuse of AIP content is subject to the terms at: http://scitation.aip.org/termsconditions. Downloaded to IP: 86.189.1.108 On: Fri, 16 May 2014 15:43:42

After broad beam cesium ion irradiation of areas of $25 \times 25\,\mu m^2$, AFM images of the irradiated surface exhibited an increased roughness up to $\sim$5 nm at a fluence of 10^{16} ions/cm^2, Fig. 2(e), but little material is removed from the surface, as expected. To study whether the irradiated layer was sufficiently amorphized to be removed by chemical etching, the samples were dipped in 2% HF for 8 min and 24% HF for 2 min. After a second round of AFM imaging to study the effects of chemical etching, the samples were electrochemically anodized for 100 ms, producing a porous silicon layer a few tens of nanometers thick. After porous silicon removal a third set of AFM images were recorded. Fig. 2(f) plots the measured depth of the irradiated regions versus fluence, after chemical etching and then after subsequent anodization. The chemically etched depth increases with fluence, as expected, with a minimum observable step of 5 nm produced for a fluence of 4×10^{13} ions/cm^2. Note that the etched depth is comparable to the ion range for fluences of 10^{16} ions/cm^2, indicating that the full irradiated volume is removed. Little change is observed at high fluences after subsequent anodization since virgin material is exposed beneath the irradiated volume. However, strong changes are observed at low fluences after anodization; the minimum fluence, which results in the formation of trench, is $\sim 4 \times 10^{11}$ ions/cm^2, two orders of magnitude lower than for chemical etching. Furthermore, the surface roughness is an order of magnitude lower than that achieved with sputtering, Fig. 2(e), and is indistinguishable from that of a virgin wafer.

Fig. 5(d) applies our anodization model to 15 keV cesium ion irradiation. At low fluences, for broad beam irradiation with longer-range 30 keV helium ions, a large diffusion current was not expected, as discussed above. Now though, under irradiation with short-range ions, chemical etching may remove the top few nanometres containing the depleted portion of the irradiated volume, allowing an enhanced diffusion current to flow towards the lower hole density at the exposed surface. Thus, for such short range ions, chemical etching superposed on anodization results in surface etching at very low fluences, well below those where chemical etching alone produces a noticeable effect. For higher fluences, the short ion range means that the irradiated depth is now thin enough to be completely removed by chemical etching. Thus, no bump is produced by depletion effects at high fluences, only an increasing etch depth due to irradiation until the irradiated depth is exceeded, at which time no further change in step eight at the irradiated regions is produced.

In summary, a comprehensive model of electrochemical anodization of p-type silicon under the influence of ion irradiation has been developed, which includes modification to the host lattice's electronic properties, and also lattice amorphization induced at high fluences, which contributes a chemical etching effect. From an electrochemical perspective, amorphous silicon wafers are considered to behave under anodization in a manner similar to high resistivity crystalline wafers.[24,25] In contrast, we have shown that ion induced amorphization introduces a more complex spectrum of effects as the amorphized layer is thin and non-uniform in depth. We further show that the anodization behaviour produced by heavy ion irradiation such as 15 keV cesium can be understood within the same model.

This work opens the way to a more widespread use of ion irradiation and electrochemical anodization across a range of ion types and energy regimes for patterning. For example, a fluence of two orders of magnitude lower than that required for sputtering is needed and an order of magnitude lower surface roughness is achieved. Furthermore, despite numerous efforts in this direction, three-dimensional nanofabrication at multi-scales of height and lateral dimensions remains highly challenging, both in terms of techniques and patterning materials. This study provides a mechanism to pattern a surface with a combination of raised features (i.e., bumps) and dips with arbitrary orientations and heights, which is an unusual capability amongst patterning and lithography processes and opens the way to make hierarchical structures and those which mimic surfaces found in nature.

We wish to thank the International Atomic Energy Agency for partial support under the CRP Project No. F11016. This work was partly performed at SSLS under NUS Core Support C-380-003-003-001, at NUSNNI under NUS Core Support C-380-000-003-001, and National Research Foundation project NRF-CRP8-2011-06.

[1] B. G. Svensson, C. Jagadish, A. Hallén, and J. Lalita, Nucl. Instrum. Methods Phys. Res. B **106**, 183 (1995).
[2] A. Hallen, N. Keskitalo, F. Masszi, and V. Nagl, J. Appl. Phys. **79**, 3906 (1996).
[3] B. G. Svensson, B. Mohadjeri, A. Hallén, J. H. Svensson, and J. W. Corbett, Phys. Rev. B **43**, 2292 (1991).
[4] M. B. H. Breese, G. W. Grime, and M. Dellith, Nucl. Instrum. Methods Phys. Res. B **77**, 332 (1993).
[5] S. Azimi, Z. Y. Dang, J. Song, M. B. H. Breese, E. Vittone, and J. Forneris, Appl. Phys. Lett. **102**, 042102 (2013).
[6] S. Azimi, J. Song, Z. Y. Dang, and M. B. H. Breese, J. Appl. Phys. **114**, 053517 (2013).
[7] V. Lehmann, *Electrochemistry of Silicon: Instrumentation, Science, Materials and Applications* (Wiley-VCH, 2002).
[8] M. J. Sailor, in *Porous Silicon in Practice* (Wiley-VCH Verlag GmbH & Co. KGaA, 2011), p. 1.
[9] J. F. Ziegler, M. D. Ziegler, and J. P. Biersack, Nucl. Instrum. Methods Phys. Res. B **268**, 1818 (2010).
[10] K. Imai, Solid-State Electron. **24**, 159 (1981).
[11] M. B. H. Breese, F. J. T. Champeaux, E. J. Teo, A. A. Bettiol, and D. J. Blackwood, Phys. Rev. B **73**, 035428 (2006).
[12] S. Azimi, M. B. H. Breese, Z. Y. Dang, Y. Yan, Y. S. Ow, and A. A. Bettiol, J. Micromech. Microeng. **22**, 015015(2012).
[13] E. J. Teo, B. Q. Xiong, Y. S. Ow, M. B. H. Breese, and A. A. Bettiol, Opt. Lett. **34**, 3142 (2009).
[14] Z. Y. Dang, M. B. H. Breese, G. Recio-Sanchez, S. Azimi, J. Song, H. Liang, A. Banas, V. Torres-Costa, and R. Martin-Palma, Nanoscale Res. Lett. **7**, 416 (2012).
[15] G. Z. Mashanovich, M. Milosevic, P. Matavulj, S. Stankovic, B. Timotijevic, P. Y. Yang, E. J. Teo, M. B. H. Breese, A. A. Bettiol and G. T. Reed, Semiconductor Sci. Technol. **23**, 064002 (2008).
[16] N. P. Economou, J. A. Notte, and W. B. Thompson, Scanning **34**, 83 (2012).
[17] U. F. Gianola, J. Appl. Phys. **28**, 868 (1957).
[18] J. F. Gibbons, E. O. Hechtl, and T. Tsurushima, Appl. Phys. Lett. **15**(4), 117 (1969).
[19] P. W. Żukowski, S. B. Kantorow, D. Mączka, and V. F. Stelmakh, Phys. Status Solidi A **112**, 695 (1989).
[20] A. D. Pearson and W. B. Harsell, Mater. Res. Bull. **7**, 567 (1972).
[21] L. Pelaz, L. A. Marqués, and J. Barbolla, J. Appl. Phys. **96**, 5947 (2004).
[22] E. C. Baranova, V. M. Gusev, Yu V. Martynenko, C. V. Starinin, and I. B. Hailbullin, in *Ion Implantation in Semiconductors and Other Materials*, edited by B. L. Crowder (Springer, New York, 1973), pp. 59.
[23] G. Bai and M.-A. Nicolet, J. Appl. Phys. **70**, 3551 (1991).
[24] R. B. Wehrspohn, J. N. Chazalviel, F. Ozanam, and I. Solomon, Thin Solid Films **297**, 5 (1997).
[25] E. Bustarret, M. Ligeon, and M. Rosenbauer, Phys. Status Solidi B **190**, 111 (1995).

This article is copyrighted as indicated in the article. Reuse of AIP content is subject to the terms at: http://scitation.aip.org/termsconditions. Downloaded to IP: 86.189.1.108 On: Fri, 16 May 2014 15:43:42